Structural and CO2 Chemisorption Analyses on Na-2(Zr1-xAlx)O-3 Solid Solutions

ARTICLE *in* THE JOURNAL OF PHYSICAL CHEMISTRY C · AUGUST 2013

Impact Factor: 4.77 · DOI: 10.1021/jp4053924

5 AUTHORS, INCLUDING:

Heriberto Pfeiffer
Universidad Nacional Autónoma de México
108 PUBLICATIONS **1,475** CITATIONS
SEE PROFILE

Brenda Alcántar-Vázquez
Universidad Nacional Autónoma de México
10 PUBLICATIONS **15** CITATIONS
SEE PROFILE

Issis Romero
Universidad Nacional Autónoma de México
15 PUBLICATIONS **125** CITATIONS
SEE PROFILE

Enrique Lima
Universidad Nacional Autónoma de México
103 PUBLICATIONS **1,046** CITATIONS
SEE PROFILE

THE JOURNAL OF PHYSICAL CHEMISTRY C

Article

pubs.acs.org/JPCC

Structural and CO_2 Chemisorption Analyses on $Na_2(Zr_{1-x}Al_x)O_3$ Solid Solutions

Brenda Alcántar-Vázquez,[†,‡] Cesar Diaz,[†] Issis C. Romero-Ibarra,[‡] Enrique Lima,[‡] and Heriberto Pfeiffer*[,‡]

[†]Facultad de Ciencias Químicas e Ingeniería, Universidad Autónoma de Baja California, Calzada Universidad #14418, Parque Industrial Internacional, Tijuana B.C. CP 22390, Mexico

[‡]Instituto de Investigaciones en Materiales, Universidad Nacional Autónoma de México, Circuito exterior s/n, Cd. Universitaria, Del. Coyoacán C.P. 04510, México DF, Mexico

ABSTRACT: Different sodium zirconate solid solutions containing aluminum ($Na_2(Zr_{1-x}Al_x)O_3$) were synthesized via a solid-state reaction. Samples were characterized using X-ray diffraction and solid-state nuclear magnetic resonance. Then, samples were tested as CO_2 captors. Characterization results show that aluminum ions can occupy zirconium or sodium sites in the Na_2ZrO_3 structure. Thus, the aluminum dissolution is compensated by different structural defects. The CO_2 capture evaluation shows that the aluminum presence into the Na_2ZrO_3 structure improves the CO_2 chemisorption within certain aluminum content under specific thermal conditions. These results were corroborated with the kinetic analysis, where the activation enthalpies were determined. The CO_2 chemisorption differences were attributed to different sodium secondary phases produced in each case and their corresponding diffusion properties. Finally, cyclic performance tests indicate that $Na_2(Zr_{1-x}Al_x)O_3$ ceramics exhibited high and stable CO_2 capture behaviors.

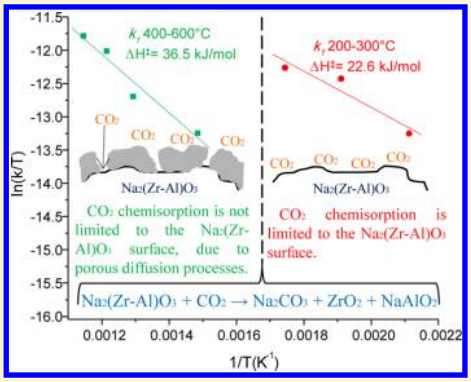

INTRODUCTION

The rapid increase in Earth's population in recent decades has led to an increase in CO_2 emissions, the main greenhouse gas. The high CO_2 levels are due to an abuse in the production and consumption of energy primarily obtained from fossil fuels.[1−3] CO_2 removal and sequestration from flue gas has been proposed as one of the most reliable solutions to mitigate global greenhouse emissions.[4] Various CO_2 capture options are available: recently solid sorbents were investigated as an innovative concept for CO_2 captors. The development of solid sorbents for CO_2 capture is an area of significance for both academic and industrial interest. The requirements for material performance to minimize the energy penalty of the capture process present a significant challenge for materials.[5]

Different alkaline ceramics, mainly lithium or sodium, show excellent CO_2 capture properties.[6−17] Among them, zirconates have been reported as good candidates as CO_2 solid sorbents. In 2004 it was reported that Na_2ZrO_3 is able to absorb CO_2 at 600 °C. Since then, several works have reported that Na_2ZrO_3 presents much better characteristics as CO_2 captor in comparison with Li_2ZrO_3.[18−20] Na_2ZrO_3 has a lamellar structure, where sodium atoms are located among the $(ZrO_3)^{2-}$ layers, which favors sodium diffusion.[17] In general, the mechanism for CO_2 chemisorption on alkaline ceramics has already been proposed. Initially, there is CO_2 chemisorption over the ceramic surface, which implies that an external shell is formed. The external shell is composed of the corresponding alkaline carbonate (Na_2CO_3), secondary phases, or metal oxides. Once the superficial CO_2 chemisorption is complete, the CO_2 chemisorption can be reactivated if the temperature is increased sufficiently to allow diffusion processes throughout the bulk of the material.[9]

Some structural, textural, and composition modifications have been performed in the alkaline ceramics to improve the kinetics of capture, the temperature ranges, and the selectivity.[19,21−24] In this sense, some alkaline ceramic solid solutions were prepared to enhance capture properties. For example, $Li_{2-x}K_xZr_2O_3$ solid solutions presented higher CO_2 absorption capacities in comparison with pure Li_2ZrO_3. The kinetic analyses indicate that $Li_{2-x}K_xZrO_3$ solid solutions can absorb CO_2 up to five times faster than Li_2ZrO_3 at short times.[25] Moreover, $Li_{4+x}(Si_{1-x}Al_x)O_4$ solid solutions were prepared to enhance lithium ion diffusion in Li_4SiO_4-based materials, at which the CO_2 chemisorption process is promoted. It was observed that the incorporation of aluminum into the Li_4SiO_4 structure highly improves the CO_2 capture properties at $T \geq 650$ °C.[17] Also, once these solid solutions react with CO_2, some secondary phases containing lithium are formed ($LiAlO_2$). It has been shown that the diffusion properties of lithium in such secondary phases may contribute to the CO_2 chemisorption.[6]

Received: May 31, 2013
Revised: July 15, 2013
Published: July 16, 2013

   dx.doi.org/10.1021/jp4053924 | J. Phys. Chem. C 2013, 117, 16483−16491

Therefore, the aim of the present work was to analyze both structural and microstructural characteristics of $Na_2(Zr_{1-x}Al_x)O_3$ solid solutions prepared via a solid-state reaction. Besides, the CO_2 chemisorption capacity and the cyclability were analyzed.

EXPERIMENTAL SECTION

Various $Na_2(Zr_{1-x}Al_x)O_3$ solid solutions were synthesized via a solid-state reaction. The solid solutions were obtained by mixing mechanically the corresponding amounts of zirconium oxide (ZrO_2, 98.0% Spectrum), sodium carbonate (Na_2CO_3, MCB lab), and aluminum nitrate ($Al(NO_3)_3{\cdot}9H_2O$, 98.0% Aldrich) with a Na/M molar ratio of 2.1:1 (M = Zr + Al) and x values between 0.05 and 0.5. Powder mixtures were subsequently calcined at 800 and 900 °C for 4 and 6 h, respectively. The solid solutions were labeled according to the substitutional element (Al) content: Al05, Al10, Al30, and Al50 correspond to the following nominal compositions $Na_2(Zr_{0.95}Al_{0.05})O_3$, $Na_2(Zr_{0.9}Al_{0.1})O_3$, $Na_2(Zr_{0.7}Al_{0.3})O_3$, and $Na_2(Zr_{0.5}Al_{0.5})O_3$, respectively. The initial Na_2ZrO_3 sample was analyzed for comparison purposes.

$Na_2(Zr_{1-x}Al_x)O_3$ solid solutions were structurally characterized using powder X-ray diffraction (XRD) and solid-state nuclear magnetic resonance (MAS NMR). The XRD patterns were obtained with a D8 Bruker diffractometer coupled to a Cu anode X-ray tube in Bragg−Brentano configuration. The Kα1 wavelength was selected with a diffracted beam Ge monochromator, and the compounds were identified conventionally using the Joint Committee Powder Diffraction Standards (JCPDS) database. The experimental error was ±5%. NMR spectra were acquired on a Bruker Avance II spectrometer with a magnetic field strength of 7.05 T, corresponding to a ^{27}Al Larmor frequency of 78.3 MHz. Short single pulses ($\pi/12$) with a recycle time of 0.5 s were used. Samples were packed into zirconia rotors of 4 mm o.d. The ^{27}Al chemical shift was expressed as ppm from an aqueous solution of $Al(NO_3)_3$ as external standard.

Different CO_2 chemisorption experiments were performed with Q500HR equipment from TA Instruments. The solid solutions were dynamically heated from room temperature to 800 at 5 °C/min. These analyses were carried out under a saturated CO_2 atmosphere. A CO_2 gas flow rate of 60 mL/min (Praxair, grade 3.0) was used in all experiments. For the isothermal analysis, the samples were initially heated to 850 °C using a N_2 flow of 60 mL/min (Praxair, grade 4.8). This initial thermal step was performed to eliminate any previous sample carbonation. Then, each sample was cooled to its respective isothermal temperature (between 300 and 700 °C) to perform independent CO_2 chemisorption processes. As the sample reached the corresponding temperature, the gas flow was switched from N_2 to CO_2. The isothermal experiments were performed using a gas flow rate of 60 mL/min throughout the duration of the experiment. To elucidate the $Na_2(Zr_{1-x}Al_x)O_3$−CO_2 capture mechanism and the corresponding microstructural properties, some products obtained from the isothermal analyses were recharacterized by XRD and N_2 adsorption. Finally, CO_2 cyclic chemisorption−desorption experiments were performed using the same thermobalance. Samples were initially heated to the specific experimental temperature under a N_2 flow. The CO_2 absorption experiments were performed at 550 and 600 °C, and the desorption processes was performed at 800 °C. After the sample reached the corresponding temperature, the gas flow was switched from N_2 to CO_2 to perform the first CO_2 chemisorption process during 30 min. After the CO_2 chemisorption, the gas flow was switched to N_2 again and the temperature was fitted to 800 °C. All of the experiments were performed using a total gas flow rate of 60 mL/min of N_2 or CO_2 throughout 20 cycles.

RESULTS AND DISCUSSION

Figure 1 shows the XRD patterns of the Na_2ZrO_3 sample and the different $Na_2(Zr_{1-x}Al_x)O_3$ solid solutions. The

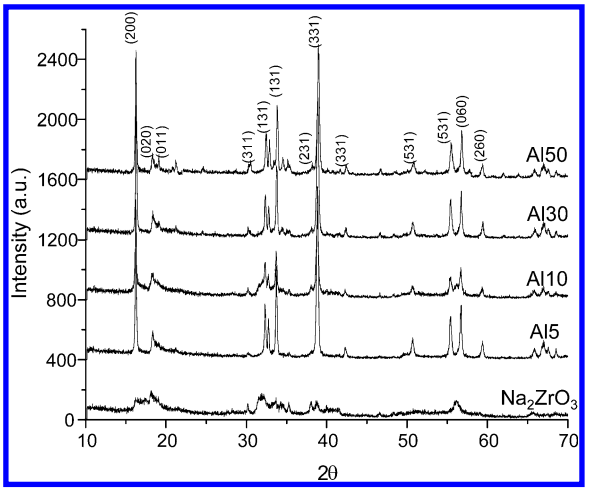

Figure 1. XRD patterns of the $Na_2(Zr_{1-x}Al_x)O_3$ solid solutions.

$Na_2(Zr_{1-x}Al_x)O_3$ solid solutions were fitted to the Na_2ZrO_3 diffraction pattern (JCPDS file 35-0770), indicating a complete aluminum dissolution up to $x \leq 0.3$. In these cases, the XRD patterns did not show any evident peak shift or intensity changes. However, if the x value was increased to 0.5, other phases were found, Na_5AlO_4 and $NaAlO_2$, indicating the aluminum solubility limit.

To corroborate the XRD results, we performed ^{27}Al MAS NMR analyses. ^{27}Al MAS NMR is the most powerful tool for investigation on the coordinative states of surface aluminum species, which are sensitive to the coordination and symmetry of the local chemical environment surrounding the aluminum nuclei.[26,27] Figure 2 displays the corresponding ^{27}Al MAS NMR spectra. It can be observed that there are two resonance peaks centered at 70−78 and 7−9 ppm, which means that the

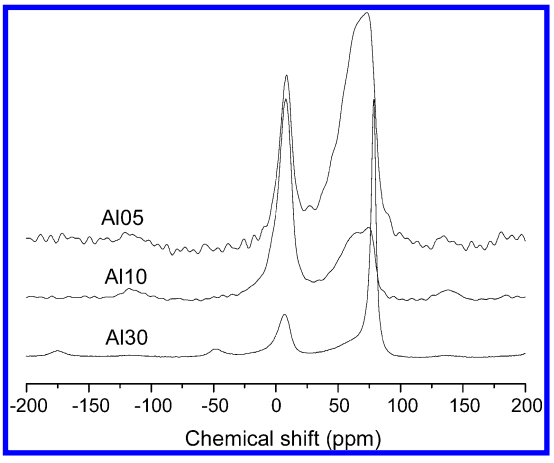

Figure 2. ^{27}Al MAS NMR of the $Na_2(Zr_{1-x}Al_x)O_3$ solid solutions.

dx.doi.org/10.1021/jp4053924 | J. Phys. Chem. C 2013, 117, 16483−16491

$Na_2(Zr_{1-x}Al_x)O_3$ structures contain two types of aluminum, tetra- and hexa-coordinated, respectively. At low aluminum concentrations (x = 0.05), the relative intensity of these two resonances is roughly the same, indicating the presence of aluminum in tetrahedral and octahedral positions. However, an augment in the aluminum percentage at 0.1 increases the intensity of the resonance peak at 9 ppm, which is associated with an increase in aluminum octahedral positions. In contrast, when it continues increasing, the percentage of aluminum at 0.3 enhances the intensity of the resonance at 78 ppm corresponding to aluminum four-fold coordinated (Al(IV)), and the presence of aluminum six-fold coordinated (Al(VI)) decreases. Figure 3 shows the Na_2ZrO_3 crystalline structure.

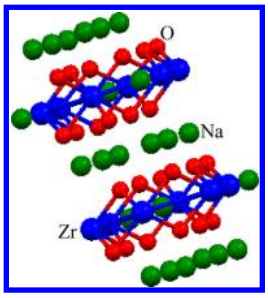

Figure 3. Scheme of the Na_2ZrO_3 crystalline structure. The spheres represent: zirconium (blue), oxygen (red), and sodium (green) atoms, respectively.

From this image, it is evident that sodium atoms occupy octahedral positions between the tetrahedral ZrO_4 layers. Initially, it could be expected that the aluminum atoms in the $Na_2(Zr_{1-x}Al_x)O_3$ solid solutions should occupy Zr tetrahedral positions. However, ^{27}Al NMR results evidenced that aluminum atoms are also located in octahedral positions, corresponding to the sodium interlayered atoms. In any case, the presence of aluminum atoms (Al^{3+}) in the tetrahedral (substituting Zr^{4+}) or the octahedral positions (substituting Na^{1+}) induces vacancy generation due to the cation charge variations. The two options are presented in reactions 1 and 2, according to the Kröger–Vink notation.

$$Na_2ZrO_3 \xrightarrow{Al_2O_3} (Na_{2-3x}Al_x)ZrO_3 \rightarrow Na_{Na} + Al^{\cdot\cdot}_{Na} + 2V'_{Na} + Zr_{Zr} + O_O \quad (1)$$

$$Na_2ZrO_3 \xrightarrow{Al_2O_3} Na_2(Zr_{1-x}Al_x)O_{3-x/2} \rightarrow Na_{Na} + Zr_{Zr} + Al'_{Zr} + 1/2V^{\cdot\cdot}_O + O_O \quad (2)$$

The possibility that aluminum does not incorporate into the Na_2ZrO_3 network and segregate as alumina has to be discarded because the intensities ratio of NMR peaks Al(IV)/Al(VI) does not correspond to the usual 1/3 that is observed for Al_2O_3.

Therefore, the presence of the aluminum atoms in these two different crystalline positions may modify the CO_2 chemisorption, as the intercrystalline sodium diffusion might be modified. This would not be the unique effect produced by the aluminum addition in the sodium zirconate phase. Another change may be related to superficial CO_2 chemisorption, as the Na_2ZrO_3 basicity can change by the aluminum addition because an amount of sodium has been displaced (see reaction 1), perhaps to the crystal borders.

To analyze the influence of the aluminum incorporation in the CO_2 capture properties of Na_2ZrO_3, we performed different experiments. Figure 4 presents the $Na_2(Zr_{1-x}Al_x)O_3$ dynamic thermograms into a CO_2 flux. The Na_2ZrO_3 sample is included for comparison purposes.

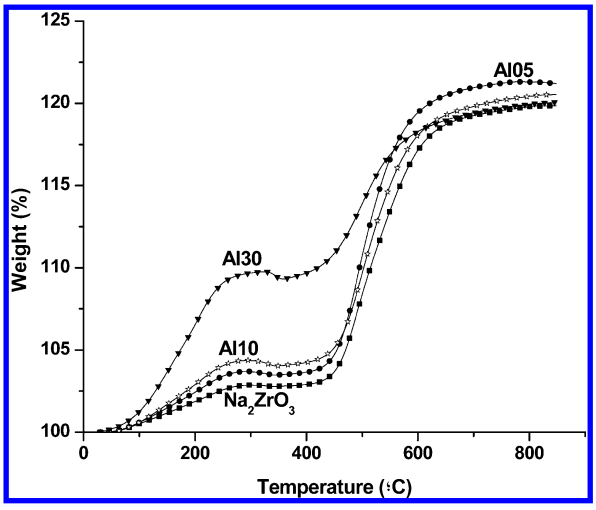

Figure 4. Thermogravimetric dynamic analyses of different $Na_2(Zr_{1-x}Al_x)O_3$ solid solutions in a flux of CO_2.

$Na_2(Zr_{1-x}Al_x)O_3$ solid solutions depicted the typical CO_2 chemisorption behavior observed for Na_2ZrO_3.[18,19,28,29] First, in the Na_2ZrO_3 case at low temperatures (30–280 °C), there is an initial CO_2 chemisorption over the particles surface, which suggests the formation of an external shell composed of Na_2CO_3 and ZrO_2. Between 285 and 400 °C there is a small desorption process (associated to the weight loss), followed by a lag period of time. These changes observed in the Na_2ZrO_3–CO_2 system correspond to a dynamic chemisorption–desorption equilibrium. Finally, at T > 400 °C, different diffusion processes are activated and the CO_2 chemisorption can continue through the bulk. The diffusion processes involve the sodium diffusion and oxygen diffusion. The oxygen diffusion is involved because part of the oxygen present in ceramics comes into the carbonate external shell.[18,28,30]

In $Na_2(Zr_{1-x}Al_x)O_3$ cases, the aluminum addition evidently enhances the superficial CO_2 chemisorption process. The weight increases from 2.8 to 9.3 wt % for Na_2ZrO_3 and Al30, respectively. This tendency corroborates that the particle surface basicity is increased by the aluminum addition. Then, between 300 and 400 °C all samples lost around 0.3 wt %, attributed to the CO_2 chemisorption–desorption equilibrium. Therefore, the superficial desorption process does not seem to be modified by the aluminum presence. After that, the CO_2 capture controlled by diffusion processes is activated at temperatures higher than 400 °C, as in the Na_2ZrO_3 sample. However, qualitatively, the aluminum addition does not seem to improve the final amount of CO_2 captured in this temperature range. It can be visualized in the Al30 weight increase slope, which apparently seems to be shorter than the others. In fact, the final weight increases varied as follows: 19.2, 20.5, 19.2, and 18.8 wt % for Na_2ZrO_3, Al05, Al10, and Al30, respectively.

To further and completely understand the CO_2 chemisorption on these ceramics, we performed different isothermal experiments (Figure 5). The $Na_2(Zr_{1-x}Al_x)O_3$ isotherms were performed between 200 and 700 °C according to the previous dynamic TG results. Figure 5A shows the Na_2ZrO_3 isotherms.

dx.doi.org/10.1021/jp4053924 | J. Phys. Chem. C 2013, 117, 16483–16491

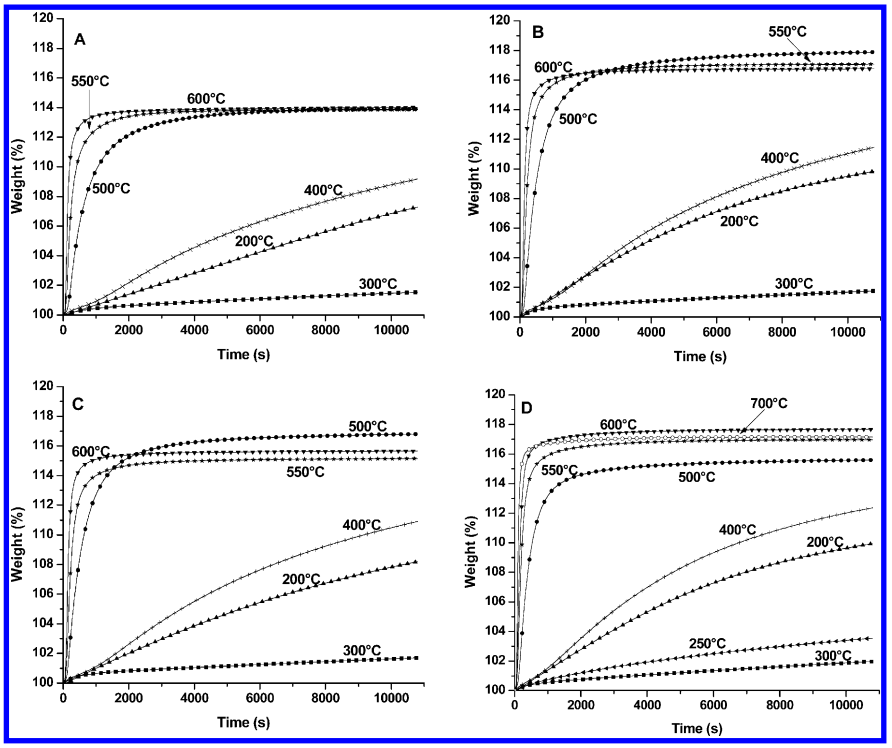

Figure 5. Isothermal analyses of the $Na_2(Zr_{1-x}Al_x)O_3$ solid solutions at different temperatures in a flux of CO_2: (A) Na_2ZrO_3, (B) Al05, (C) Al10, and (D) Al30.

At the lowest temperature (200 °C), the isotherm showed an exponential behavior, which did not reach the plateau after 180 min. Na_2ZrO_3 absorbed 7.3 wt %, which is in good agreement with previous reports.[18] This process has been associated with CO_2 chemisorption mainly produced on the surface of the Na_2ZrO_3 particles. At this point, a thin Na_2CO_3–ZrO_2 shell should be produced over the Na_2ZrO_3 particle surfaces. However, at 300 °C, CO_2 chemisorption was more minor than that previously observed at 200 °C. At this temperature, the CO_2 chemisorption was only 1.5 wt % after 3 h. Similar atypical behaviors have been reported for the CO_2 chemisorption on other alkaline ceramics such as Li_5AlO_4, Li_2ZrO_3, and Li_2CuO_2.[7,31,32] This behavior has been associated with a sintering process produced during the heating of the samples, which produces an important decrement of the surface area. However, this phenomenon is usually observed at higher temperatures ($T \geq 500$ °C) once different diffusion processes are activated. If this temperature (300 °C) is analyzed in the dynamic thermograms (see Figure 4), it corresponds to the CO_2 desorption activation temperature. Therefore, at 300 °C, the CO_2 chemisorption is significantly reduced because there is a superficial chemisorption–desorption equilibrium and not because of a particle sintering effect. At 400 °C, the quantity of CO_2 captured increased again. Here the weight increase was 9.2 wt %. It may be associated with the CO_2 diffusion through the Na_2CO_3–ZrO_2 mesoporous external shell.[28] In the isothermal analyses performed between 500 and 600 °C, the final weight gained was almost the same, but the CO_2 reaction was faster at higher temperatures. It is evident that CO_2 chemisorption at short times dramatically increased as a function of the temperature because after the first minutes it had captured almost the entire final weight gained (14 wt %). At those temperatures, the chemisorption was very fast; actually, the exponential curves reached their plateau in a few minutes (20 min, at 600 °C). These results confirm that $T \geq 500$ °C does not improve CO_2 capture but kinetics.

The Al05 isotherms show similar behavior as Na_2ZrO_3 (Figure 5B). Al05 shows a slightly increase in the CO_2 chemisorption at all temperatures. The main difference observed in this sample occurred between 500 and 600 °C. In this temperature range, the sample treated at 500 °C was the sample that gained more weight (17.8 wt %). At higher temperatures the final weight decreased up to 16.4 wt % at 600 °C. In this case, the sintering process described above did produce this isothermal behavior. Similar effects were already reported to Na_2ZrO_3[28] and other alkaline ceramics,[7,31,32] where it was described for the Na_2ZrO_3 that the Na_2CO_3–ZrO_2 external shell sinters at $T \geq 550$ °C.

The Al10 isotherms (Figure 5C) presented exactly the same exponential behavior as those observed in the Na_2ZrO_3 and Al05 samples. Nevertheless, Al30 solid-solution sample produced some specific variations in the isotherms (Figure 5D). At low temperatures (200–400 °C), the behavior did not vary in comparison with samples previously described. In fact, an isotherm experiment performed at 250 °C was included, which confirmed the atypical behavior presented between 200 and 300 °C. However, at high temperatures, a different behavior is observed with respect to the previous samples. The highest CO_2 capture was not produced at 500 °C, as in the Al05 and Al10 samples. In the Al30 sample, the maximum CO_2 capture was obtained at 600 °C (17.7 wt %), while the sintering effect was detected only at $T \geq 600$ °C. Apparently, high aluminum additions inhibit the sintering process.

To confirm the above and continue understanding the CO_2 chemisorption of the $Na_2(Zr_{1-x}Al_x)O_3$ solid solutions, some $Na_2(Zr_{1-x}Al_x)O_3$–CO_2 isothermal products were recharacterized using XRD. The Al30-CO_2 isothermal product, obtained at 600 °C, was analyzed using XRD. As it is shown in Figure 6, the

dx.doi.org/10.1021/jp4053924 | J. Phys. Chem. C 2013, 117, 16483–16491

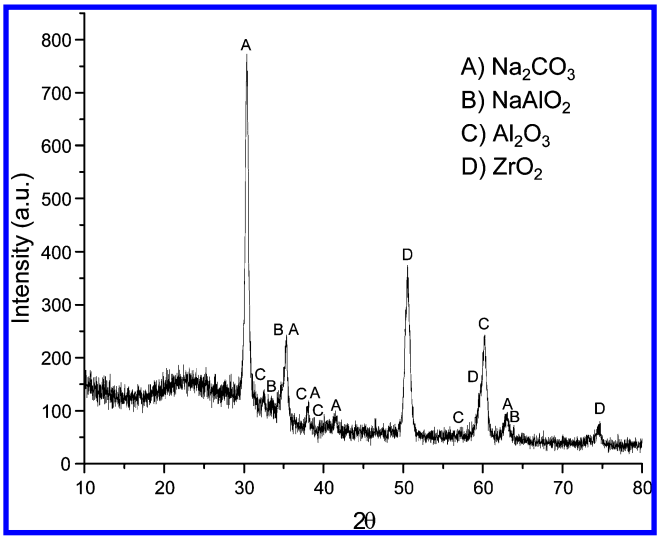

Figure 6. XRD pattern of the Al30-CO_2 sample products obtained from the isothermal experiment performed at 600 °C.

presence of Na_2CO_3 was observed in the sample, which corresponds to the main product obtained during the CO_2 chemisorption on the $Na_2(Zr_{1-x}Al_x)O_3$−CO_2 solid solutions. In addition, other secondary phases were also identified; ZrO_2, Al_2O_3, and $NaAlO_2$. It must be mentioned that the amorphous phase detected in the diffractogram corresponds to the glass support; because the isothermal products are small quantities it was not possible to eliminate this signal. Previous reports showed that the external shell plays a significant role in the diffusion process because the CO_2 chemisorption process can be enhanced or limited depending on the diffusion coefficients of the secondary phases.[6,33] For example, previous work reported that $LiAlO_2$ presence enhances the lithium diffusion at $T > 600$ °C.[6] The activation enthalpy for lithium diffusion in $LiAlO_2$ is 0.77 eV,[34] while the activation enthalpy for sodium diffusion in NaO_2-$11Al_2O_3$ is 0.17 eV (both calculated between 400 and 700 °C).[35] Thus, the activation enthalpy for sodium diffusion is smaller than the lithium one. So, it might be assumed that the $NaAlO_2$ presence in the external shell may enhance the sodium diffusion at temperatures close to 600 °C.

To compare the temperature effect in the solid−solution samples, Figure 7 shows some of the $Na_2(Zr_{1-x}Al_x)O_3$ isothermal experiments as a function of the aluminum content at specific temperatures (400, 500, 550, and 600 °C). At 400 °C, none of the samples reached the plateau, and the CO_2 captured increases as a function of the aluminum content. Al30 provides the maximum capture with 12.4 wt %. It means 3.2 wt % more than Na_2ZrO_3. A completely different behavior is observed at 500 °C or higher temperatures, where the diffusion processes had been activated and all samples reached the plateau during the first minutes. The samples containing aluminum chemisorbed more CO_2 than Na_2ZrO_3. In fact, Na_2ZrO_3 is the sample that chemisorbed CO_2 at a slower rate in comparison with the three solid solutions. In the first 10 min, Al05, Al10, and Al30 chemisorb 10.2, 9.3, and 10.8 wt %, respectively, while Na_2ZrO_3 just absorbed 7.0 wt %. A similar behavior was produced at 550 °C. After only 8 min, the samples captured between 10 and 14 wt % of CO_2. The final weight gained in Al05 and Al30 is the same (17 wt %). However, the

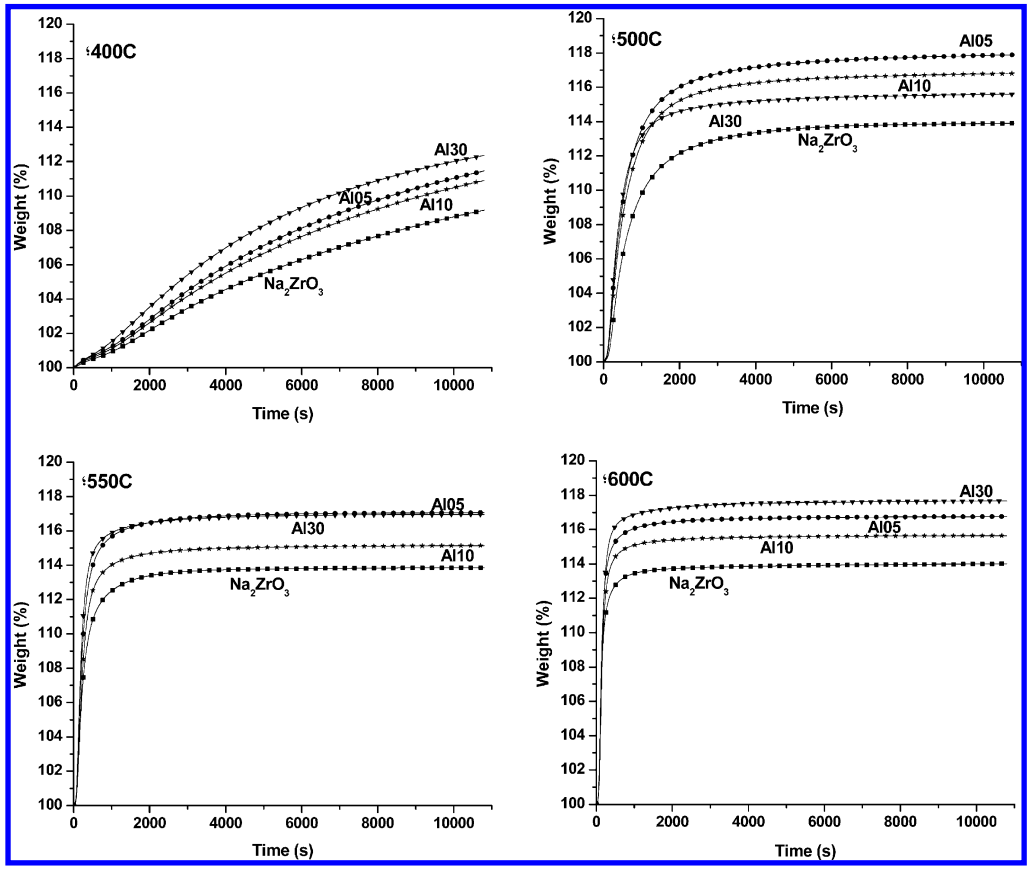

Figure 7. Kinetic isotherms performed of the $Na_2(Zr_{1-x}Al_x)O_3$ solid solutions at different temperatures (400, 500, 550, and 600 °C) in a flux of CO_2.

dx.doi.org/10.1021/jp4053924 | J. Phys. Chem. C 2013, 117, 16483−16491

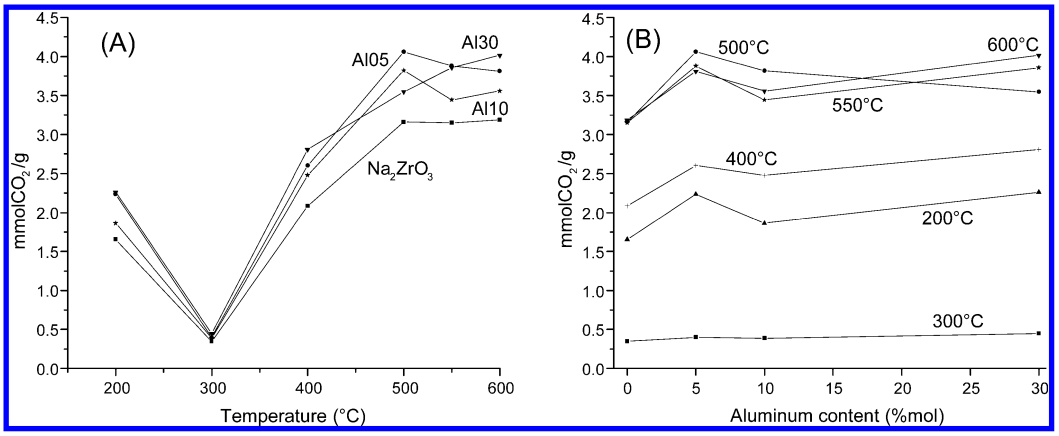

Figure 8. Comparison of the maximum CO_2 capture trends in the different $Na_2(Zr_{1-x}Al_x)O_3$ solid solutions as a function of temperature (A) or aluminum content (B).

Table 1. Kinetic Parameters of Al30 Isotherms Fitted to Double or Triple Exponential Models

T (°C)	A	B	D	C_1 or C_2	k_1 (s^{-1})	k_2 (s^{-1})	k_3 (s^{-1})	R^2
200	−0.9650	−0.0571	−14.6604	113.73	8.30 x10^{-04}	−2.30 × 10^{-04}	1.40 × 10^{-04}	0.99998
250	−0.3194	−5.4548	−1.0794	106.83	2.09 × 10^{-03}	5.00 × 10^{-05}	2.30 × 10^{-04}	0.99997
300	−0.4126	−2.7074	−2.8431	105.98	2.70 × 10^{-03}	3.00 × 10^{-05}	3.00 × 10^{-05}	0.99997
400	2.6465	−7.0431	−10.6001	115.18	1.19 × 10^{-03}	1.00 × 10^{-04}	2.70 × 10^{-04}	0.99997
500	−16.6521	−1.4262		115.72	2.37x 10^{-03}	2.40 × 10^{-04}		0.99559
550	−19.3023	−1.2314		116.98	4.99 × 10^{-03}	4.50 × 10^{-04}		0.98848
600	−20.9796	−0.9309		117.68	6.64 × 10^{-03}	3.90 × 10^{-04}		0.98355

chemisorption rate seems to be different because after the first 8 min Al05 reached 80.6% of its efficiency, while Al30 presented 85.5% as its final efficiency. Finally, the isotherms at 600 °C do not improve the CO_2 capture in Na_2ZrO_3 and Al05, while in Al10 and Al30 the increase is minimal compared with that obtained at 550 °C (3.3 and 4.1 wt % in Al10 and Al30, respectively).

All of these results are summarized in Figure 8, in which the final weight increases are presented in millimoles of CO_2 captured per gram of $Na_2(Zr_{1-x}Al_x)O_3$ solid solution (mmol/g) as a function of the temperature or the aluminum content. Once the results are compared as a function of the aluminum content (Figure 8B), it is evident that $Na_2(Zr_{1-x}Al_x)O_3$ solid solutions chemisorbed more CO_2 than Na_2ZrO_3 at all temperatures, although there is not a clear tendency among the Al-containing samples. Something else must be pointed out from this curve: at 300 °C, the CO_2 chemisorption is decreased due to the CO_2 chemisorption−desorption equilibrium established in the particle surfaces.

To explain the CO_2 capture increases observed in the Al-containing samples, we must take into account the following factors, dividing the aluminum effect in two different temperature ranges: at moderate temperatures (400−550 °C) and high temperatures (600−700 C). In the high-temperature range, the formation of vacancies during synthesis should favor some intercrystalline diffusion processes. Additionally, the presence of aluminum modifies the external shell composition as follows: Na_2CO_3−ZrO_2−$NaAlO_2$−Al_2O_3, where the $NaAlO_2$ and Al_2O_3 contents increase as a function of the aluminum present in the solid solutions. Therefore, the sodium intercrystalline diffusion probably enhances at temperatures close to 600 °C. Conversely, at moderate temperatures the external shell mesoporosity decreased with the aluminum content, limiting the CO_2 diffusion. The aluminum content tends to reduce the sintering process, allowing a higher CO_2 chemisorption at high temperatures.

After the qualitative analysis, isotherms were fitted to double- (eq 3) or triple- (eq 4) exponential models, as there are two or three different processes taking place: CO_2 chemisorption over the $Na_2(Zr_{1-x}Al_x)O_3$ surface of the particles (process 1), which indicates the formation of an external shell of alkaline carbonate, the CO_2 chemisorption kinetically controlled by diffusion processes (process 2), and in some cases, CO_2 desorption process is presented (process 3).[7−9,18,30,35−37] The double- and triple-exponential models were defined by the following equations:

$$y = A\ \exp^{-k1t} + B\ \exp^{-k2t} + C_1 \quad (3)$$

$$y = A\ \exp^{-k1t} + B\ \exp^{-k2t} - D\ \exp^{-k3t} + C_2 \quad (4)$$

where y represents the weight percentage of CO_2 chemisorbed, t is the time, and k_1, k_2, and k_3 are the exponential constants for the CO_2 chemisorption over the surface of the $Na_2(Zr_{1-x}Al_x)$-O_3 particles, the CO_2 chemisorption kinetically controlled by diffusion processes, and the CO_2 desorption, respectively. Additionally, the pre-exponential factors A, B, and D indicate that the intervals during each process control the whole CO_2 chemisorption−desorption process, and the C_1 and C_2 constants indicate the y intercept of the two different models, respectively.

Isothermal experiments at temperatures between 200 and 400 °C were fitted to the triple exponential models, and the isotherms between 500 and 600 °C were fitted to double-exponential model, assuming that the CO_2 desorption is negligible in this temperature range. The kinetics parameters, pre-exponential constants, and R^2 values obtained in Al30 at each temperature are presented in Table 1. (The other samples were also fitted, but these data are not shown.) It can be seen

dx.doi.org/10.1021/jp4053924 | J. Phys. Chem. C 2013, 117, 16483−16491

that k_1 values are, in general, one or two orders of magnitude higher than those obtained for the k_2, in agreement with previous reports.[18,28,30,33,38] Thus, the CO_2 chemisorption process controlled by diffusion processes is the limiting step of the whole reaction process. Additionally, the CO_2 desorption constant values (k_3) are always smaller than direct CO_2 chemisorption (k_1) but similar to CO_2 chemisorption kinetically controlled by diffusion processes (k_2). These results confirm the qualitative description given above about the equilibrium chemisorption−desorption observed at low temperatures.

Moreover, the A values are smaller than B values at low temperatures (200−400 °C). However, at high temperatures ($T \geq 500$ °C) this trend is reversed. In other words, the B values became smaller. This behavior has already been reported during the CO_2 capture in other alkaline solid solutions, $Li_{4+x}(Si_{1-x}Al_x)O_4$.[33] At low temperatures ($T \leq 500$ °C), the external shell is mesoporous, and thus the CO_2 chemisorption process was not limited to the bulk diffusion processes. However, at temperatures higher than 500 °C, the external shell probably sinters and the porosity disappears. In this case, CO_2 is not able to diffuse through the porous external shell. Therefore, the CO_2 chemisorption must be controlled by intercrystalline sodium diffusion processes.

To analyze the temperature and the aluminum content dependence of the different processes, we used the Eyring's model (eq 5)

$$\ln(k/T)) = -(\Delta H^{\ddagger}/R)(1/T) + \ln E + \Delta S^{\ddagger}/R \qquad (5)$$

where k is the rate constant value; E represents a preexponential factor, which in Eyring's formulation is equal to the ratio of Boltzmann's constant to Planck's constant; R is the ideal gas constant; and $\Delta H^{\ddagger}$ and $\Delta S^{\ddagger}$ are the activation enthalpy and entropy, respectively.

Although the three sets of constant values were fitted to Eyring's model, only the CO_2 direct chemisorption (k_1) and CO_2 chemisorption kinetically controlled by diffusion processes (k_2) presented a linear behavior (Figure 9). In the k_3 case, the values obtained did not present any specific trend. The CO_2 direct chemisorption process presents two different linear trends, one at moderate temperatures (200−400 °C) and the other at high temperatures (400−600 °C). Thus, the $\Delta H^{\ddagger}$ of CO_2 direct chemisorption determined was equal to 22.6 and 36.6 kJ/mol for low- and high-temperature ranges, respectively. These results show that CO_2 direct chemisorption is more dependent on the temperature at $T \geq 400$ °C. Also, the $\Delta H^{\ddagger}$ of CO_2 chemisorption kinetically controlled by diffusion processes (at 400−600 °C) was 30.6 kJ/mol; less dependent on temperature than CO_2 direct chemisorptions at the same temperature range.

Figure 10 shows the $\Delta H^{\ddagger}$ values of CO_2 direct chemisorption and CO_2 chemisorption kinetically controlled by diffusion processes as a function of aluminum content between 400 and 600 °C. These results clearly showed that the $\Delta H^{\ddagger}$ values obtained for CO_2 chemisorption kinetically controlled by diffusion processes were always less than CO_2 direct chemisorptions (except in Na_2ZrO_3). Namely, CO_2 chemisorption kinetically controlled by diffusion processes was less dependent on temperature that CO_2 direct chemisorption. Moreover, CO_2 direct chemisorption presents linear behavior; the CO_2 chemisorption is proportional to the aluminum content (until $x = 0.10$). In contrast, CO_2 chemisorption kinetically controlled by diffusion processes did not present any specific trend. It appears that CO_2 direct chemisorption becomes more dependent on temperature as a function of aluminum content when $x \leq 0.10$.

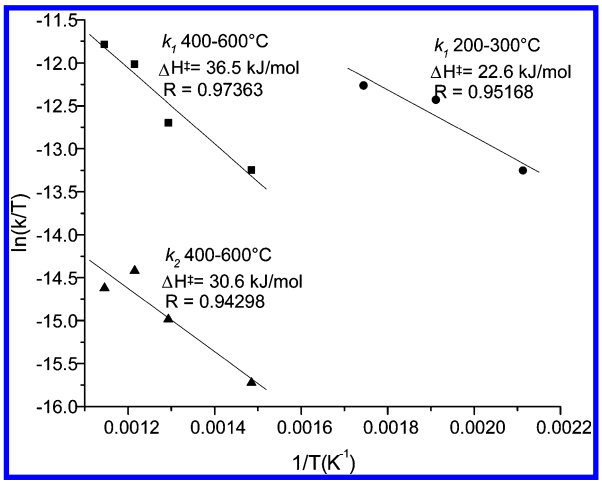

Figure 9. Eyring's plots for the k_1 (CO_2 direct chemisorption) and k_2 (CO_2 chemisorption kinetically controlled by diffusion processes) constant values for Al30.

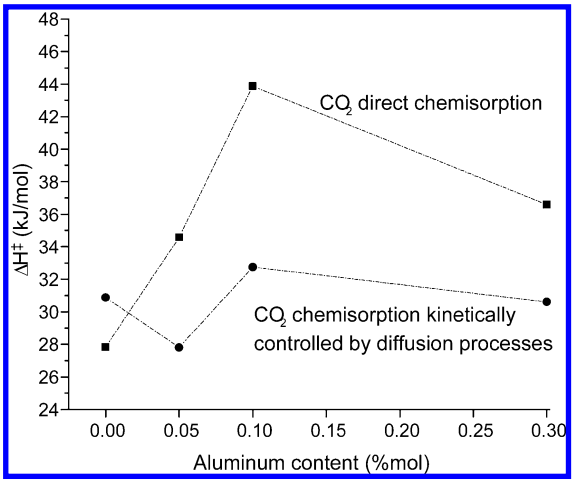

Figure 10. Plot of the $\Delta H^{\ddagger}$ values of both processes (k_1 and k_2) as a function of aluminum content. Data obtained using the isotherms between 400 and 600 °C.

To evaluate the regeneration properties and the thermal stability after several cycles of CO_2 chemisorption/desorption in the $Na_2(Zr_{1-x}Al_x)O_3$ solid solutions, we tested Al05 and Al30 samples using a multicycle method. The cyclic behavior was analyzed at 550 and 600 °C for Al05 and Al30, respectively, because these temperatures obtained the highest CO_2 chemisorptions, respectively. Figure 11 shows the CO_2 chemisorption/desorption multicycle performance of Al05 and Al30. The result for Al05 indicates that the CO_2 chemisorption capacity reaches ~17.6 wt % for the first cycle, and after 20 cycles, the CO_2 chemisorption capacity increases and stabilizes to 19.1 wt %. In contrast, for Al30, the CO_2 chemisorption in the first cycle was 18.4 wt %, but after 20 cycles, its capacity decreased to 16.3 wt % (Figure 11-B). The samples showed a different behavior during the performance of several cycles. In fact, Al05 shows a slight drop in the CO_2

dx.doi.org/10.1021/jp4053924 | J. Phys. Chem. C 2013, 117, 16483−16491

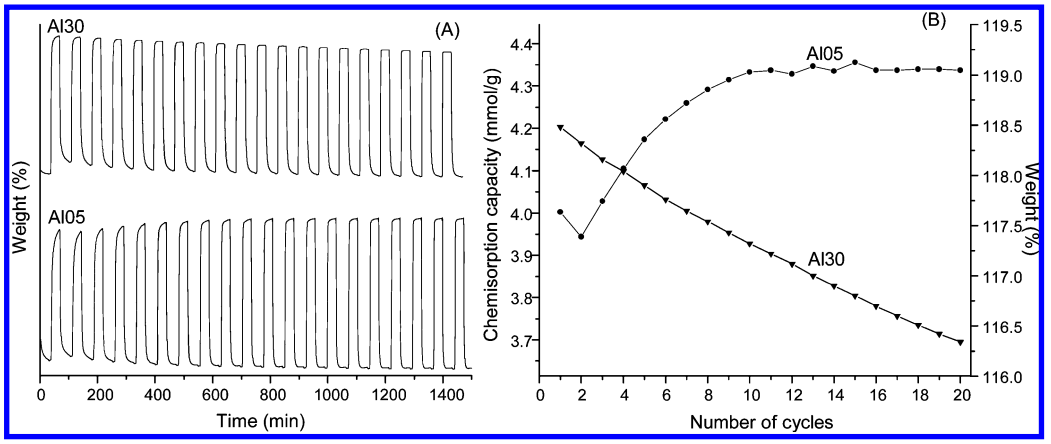

Figure 11. Multicycle performance of CO_2 chemisorption/desorption on Al05 and Al30, where the CO_2 absorptions were performed at 550 and 600 °C for 30 min, respectively (A). Desorption process was performed at 800 °C under a N_2 flow. Cyclic stability of the samples is presented in weight percentage and millimoles of CO_2 per gram of sample (B).

chemisorption in cycle number two but continues to rise again until the cycle number 9. after which it is kept constant. In contrast, in Al30, the CO_2 chemisorption decreased gradually after each cycle. This behavior may be related to the difference in the mesoporosity of the materials in this temperature range or to aluminum rearrangements. It was previously mentioned that the external shell mesoporosity decreased with the aluminum content, limiting the CO_2 diffusion. Additionally, a small loss of weight of the Al30 sample was observed during the multicycle process, perhaps by the Na_2O sublimation produced during desorption process, which may also result in a reduction in the CO_2 chemisorption capacity.

CONCLUSIONS

$Na_2(Zr_{1-x}Al_x)O_3$ solid solutions were synthesized via a solid-state reaction and then characterized using XRD and MAS NMR. These analyses proved that aluminum atoms are incorporated into the Na_2ZrO_3 structure, occupying zirconium and sodium atom sites. $Na_2(Zr_{1-x}Al_x)O_3$ were able to chemisorb CO_2 in a wide temperature range (200−700 °C), exhibiting higher CO_2 chemisorptions than Na_2ZrO_3. During the isothermal analysis, the solid solutions sintered between 200 and 300 °C, producing an important decrease in the surface area and the CO_2 chemisorption. Isotherms were fit to double or triple exponential models: (1) the CO_2 chemisorption over the surface of the $Na_2(Zr_{1-x}Al_x)O_3$ particles, (2) the CO_2 chemisorption kinetically controlled by diffusion processes, and (3) the CO_2 desorption process. The last process was detected only between 200 and 400 °C. The kinetic constant values indicated that the CO_2 chemisorption kinetically controlled by diffusion processes is the rate-limiting step for the whole process. Additionally, $\Delta H^{\ddagger}$ values tended to increase as a function of the aluminum content. The cyclic experiments indicate that Al05 solid solution presents high and stable behaviors.

AUTHOR INFORMATION

Corresponding Author

*Phone: +52 (55) 5622 4627. Fax: +52 (55) 56161371. E-mail: pfeiffer@iim.unam.mx.

Notes

The authors declare no competing financial interest.

ACKNOWLEDGMENTS

This work was financially supported by the projects SENER-CONACYT 150358 and PAPIIT-UNAM IN-102313. B.A.-V. thanks CONACYT for financial support. We thank Adriana Tejeda for technical help.

REFERENCES

(1) Reddy, E. P.; Smirniotis, P. G. High-Temperature Sorbents for CO_2 Made of Alkali Metals Doped on CaO Supports. *J. Phys. Chem. B* **2004**, *108*, 7794−7800.

(2) Lee, K. B.; Beaver, M. G.; Caram, H. S.; Sircar, S. Reversible Chemisorbents for Carbon Dioxide and Their Potential Applications. *Ind. Eng. Chem. Res.* **2008**, *47*, 8048−8062.

(3) Schrag, D. P. Confronting the Climate-Energy Challenge. *Elements* **2007**, *3*, 171−178.

(4) *Advances in CO_2 Conversion and Utilization*; Yun-Hang, H., Ed.; ACS Symposium Series 1056; American Chemical Society: Washington, DC, 2010.

(5) Drage, T. C.; Snape, C. E.; Stevens, L. A.; Wang, J. W.; Cooper, A. I.; Dawson, R.; Guo, X.; Satterley, C.; Irons, R. Materials Challenges for the Development of Solid Sorbents for post-Combustion Carbon Capture. *J. Mater. Chem.* **2012**, *22*, 2815−2823.

(6) Ortiz-Landeros, J.; Ávalos-Rendón, T. L.; Gómez-Yáñez, C.; Pfeiffer, H. Analysis and Perspectives Concerning CO_2 Chemisorption on Lithium Ceramics Using Thermal Analysis. *J. Therm. Anal. Calorim.* **2012**, *108*, 647−655.

(7) Ávalos-Rendón, T.; Casa-Madrid, J.; Pfeiffer, H. Thermochemical Capture of Carbon Dioxide on Lithium Aluminates ($LiAlO_2$ and Li_5AlO_4): A New Option for the CO_2 Absorption. *J. Phys. Chem. A* **2009**, *113*, 6919−6923.

(8) Mejia-Trejo, V. L.; Fregoso-Israel, E.; Pfeiffer, H. Textural, Structural, and CO_2 Chemisorption Effects Produced on the Lithium Orthosilicate by Its Doping with Sodium ($Li_{4-x}Na_xSiO_4$). *Chem. Mater.* **2008**, *20*, 7171−7176.

(9) Mosqueda, H. A.; Vazquez, C.; Bosch, P.; Pfeiffer, H. Chemical Sorption of Carbon Dioxide (CO_2) on Lithium Oxide (Li_2O). *Chem. Mater.* **2006**, *18*, 2307−2310.

(10) Nair, B. N.; Burwood, R. P.; Goh, V. J.; Nakagawa, K.; Yamaguchi, T. Lithium Based Ceramics Materials and Membranes for High Temperature CO_2 Separation. *Prog. Mater. Sci.* **2009**, *54*, 511−541.

(11) Gauer, C.; Heschel, W. Doped Lithium Orthosilicate for Absorption of Carbon Dioxide. *J. Mater. Sci.* **2006**, *41*, 2405−2409.

(12) Olivares-Marín, M.; Castro-Díaz, M.; Drage, T. C.; Maroto-Valer, M. M. Use of Small-Amplitude Oscillatory Shear Rheometry to Study the Flow Properties of Pure and Potassium-Doped Li_2ZrO_3

Sorbents During the Sorption of CO_2 at High Temperatures. *Sep. Purif. Technol.* **2010**, *73*, 415−420.
(13) Pacciani, R.; Torres, J.; Solsona, P.; Coe, C.; Quinn, R.; Hufton, J.; Golden, T.; Vega, L. F. Influence of the Concentration of CO_2 and SO_2 on the Absorption of CO_2 by a Lithium Orthosilicate-Based Absorbent. *Environ. Sci. Technol.* **2011**, *45*, 7083−7088.
(14) Xiao, Q.; Tang, X.; Liu, Y.; Zhong, Y.; Zhu, W. Citrate Route to Prepare K-Doped Li_2ZrO_3 Sorbents with Excellent CO_2 Capture Properties. *Chem. Eng. J.* **2011**, *174*, 231−235.
(15) Xiao, Q.; Liu, Y.; Zhong, Y.; Zhu, W. A Citrate Sol-Gel Method to Synthesize Li_2ZrO_3 Nanocrystals with Improved CO_2 Capture Properties. *J. Mater. Chem.* **2011**, *21*, 3838−3842.
(16) Rodríguez-Mosqueda, R.; Pfeiffer, H. Thermokinetic Analysis of the CO_2 Chemisorption on Li_4SiO_4 by Using Different Gas Flow Rates and Particle Sizes. *J. Phys. Chem. A* **2010**, *114*, 4535−4541.
(17) Ortiz-Landeros, J.; Gomez-Yañez, C.; Palacios-Romero, L. M.; Lima, E.; Pfeiffer, H. Structural and Thermochemical Chemisorption of CO_2 on $Li4_{+x}(Si_{1-x}Al_x)O_4$ and $Li_{4-x}(Si_{1-x}V_x)O_4$ Solid Solutions. *J. Phys. Chem. A* **2012**, *116*, 3163−3171.
(18) Alcerreca-Corte, I.; Fregoso-Israel, E.; Pfeiffer, H. CO_2 Absorption on Na_2ZrO_3: A Kinetic Analysis of the Chemisorption and Diffusion Processes. *J. Phys. Chem. C* **2008**, *112*, 6520−6525.
(19) Pfeiffer, H.; Vazquez, C.; Lara, V. H.; Bosch, P. Thermal Behavior and CO_2 Absorption of $Li_{2-x}Na_xZrO_3$ Solid Solutions. *Chem. Mater.* **2007**, *19*, 922−926.
(20) Zhao, T.; Ochoa-Fernández, E.; Rønning, M.; Chen, D. Preparation and High-Temperature CO_2 Capture Properties of Nanocrystalline Na_2ZrO_3. *Chem. Mater.* **2007**, *19*, 3294−3301.
(21) Seggiani, M.; Puccini, M.; Vitolo, S. Alkali Promoted Lithium Orthosilicate for CO_2 Capture at High Temperature and Low Concentration. *Int. J. Greenhouse Gas Control* **2013**, *17*, 25−31.
(22) Pfeiffer, H.; Lima, E.; Bosch, P. Lithium-Sodium Metazirconate Solid Solutions, $Li_{2-x}Na_xZrO_3$ ($0 \leq x \leq 2$): A Hierarchical Architecture. *Chem. Mater.* **2006**, *18*, 2642−2647.
(23) Nikulshina, V.; Ayesa, N.; Gálvez, M. E.; Steinfeld, A. Feasibility of Na-Based Thermochemical Cycles for the Capture of CO_2 from Air-Thermodynamic and Thermogravimetric Analyses. *Chem. Eng. J.* **2008**, *140*, 62−70.
(24) Khokhani, M.; Khomane, R. B.; Kulkarni, B. D. Sodium-Doped Lithium Zirconate Nano-Squares: Synthesis, Characterization and Applications for CO_2 Sequestration. *J. Sol-Gel Sci. Technol.* **2012**, *61*, 316−320.
(25) Veliz-Enriquez, M. Y.; Gonzalez, G.; Pfeiffer, H. Synthesis and CO_2 Capture Evaluation of $Li_{2-x}K_xZrO_3$ Solid Solutions and Crystal Structure of a New Lithium-Potassium Zirconate Phase. *J. Solid State Chem.* **2007**, *180*, 2485−2492.
(26) Fyfe, C. A.; Gobbi, G. C.; Klinowski, J.; Thomas, J. M.; Ramdas, S. Resolving Crystallographically Distinct Tetrahedral Sites in Silicalite and ZSM-5 by Solid-State NMR. *Nature* **1982**, *296*, 530−533.
(27) Engelhardt, G.; Michel, D. *High-Resolution Solid-State NMR of Silicates and Zeolites*; Wiley: New York, 1987; p488.
(28) Martínez-dlCruz, L.; Pfeiffer, H. Microstructural Thermal Evolution of the Na_2CO_3 Phase Produced during a Na_2ZrO_3−CO_2 Chemisorption Process. *J. Phys. Chem.* **2012**, *116*, 9675−9680.
(29) Santillan-Reyes, G. G.; Pfeiffer, H. Analysis of the CO_2 Capture in Sodium Zirconate (Na_2ZrO_3). Effect of the Water Vapor Addition. *Int. J. Greenhouse Gas Control* **2011**, *5*, 1624−1629.
(30) Martínez-dlCruz, L.; Pfeiffer, H. Effect of Oxygen Addition on the Thermokinetic Properties of CO_2 Chemisorption on Li_2ZrO_3. *Ind. Eng. Chem. Res.* **2010**, *49*, 9038−9042.
(31) Iwana, A.; Stephensonb, H.; Ketchiec, C.; Lapkina, A. High Temperature Sequestration of CO_2 Using Lithium Zirconates. *Chem. Eng. J.* **2009**, *146*, 249−258.
(32) Palacios-Romero, L. M.; Lima, E.; Pfeiffer, H. Structural Analysis and CO_2 Chemisorption Study on Nonstoichiometric Lithium Cuprates ($Li_{2+x}CuO_{2+x/2}$). *J. Phys. Chem. A.* **2009**, *113*, 193−198.
(33) Ortiz-Landeros, J.; Romero-Ibarra, I. C.; Gomez-Yañez, C.; Lima, E.; Pfeiffer, H. $Li_{4+x}(Si_{1-x}Al_x)O_4$ Solid Solution Mechanosynthesis and Kinetic Analysis of the CO_2 Chemisorption Process. *J. Phys. Chem. A* **2013**, *117*, 6303−6311.
(34) Matsuo, T.; Ohno, H.; Noda, K.; Konishi, S.; Yoshida, H.; Watanabe, H. Nuclear Magnetic Resonance Investigations of Lithium Diffusion in Li_2O, Li_2SiO_3 and $LiAlO_2$. *J. Chem. Soc., Faraday Trans.* **1983**, *79*, 1205−1216.
(35) Imai, A.; Harata, M. Ionic Conduction of Impurity-Doped β-Alumina Ceramics. *Jpn. J. Appl. Phys.* **1972**, *11*, 180−185.
(36) Shan, S. Y.; Jia, Q. M.; Jiang, L. H.; Li, Q. C.; Wang, Y. M.; Peng, J. H. Novel Li_4SiO_4-Based Sorbents from Diatomite for High Temperature CO_2 Capture. *Ceram. Int.* **2013**, *39*, 5437−5441.
(37) Qi, Z.; Daying, H.; Yang, L.; Qian, Y.; Zibin, Z. Analysis of CO_2 Sorption/Desorption Kinetic Behaviors and Reaction Mechanism on Li_4SiO_4. *AIChE J.* **2013**, *59*, 901−911.
(38) Ávalos-Rendon, T.; Lara, V. H.; Pfeiffer, H. CO_2 Chemisorption and Cyclability Analyses of Lithium Aluminate Polymorphs (α-and β-Li_5AlO_4). *Ind. Eng. Chem. Res.* **2012**, *51*, 2622−2630.